Supplement of Atmos. Chem. Phys., 19, 13945–13956, 2019
https://doi.org/10.5194/acp-19-13945-2019-supplement

Atmospheric Chemistry and Physics
Open Access
EGU

Supplement of

Molecular characterization of polar organic aerosol constituents in off-road engine emissions using Fourier transform ion cyclotron resonance mass spectrometry (FT-ICR MS): implications for source apportionment

Min Cui et al.

Correspondence to: Yingjun Chen (yjchenfd@fudan.edu.cn), Jun Li (junli@gig.ac.cn), and Junyu Zheng (zhengjunyu_work@hotmail.com)

S1: Analysis of TOC and optical properties for water and 90%DCM+10%MeOH extractions

One portions of water and 90%DCM+10%MeOH extractions were obtained to analyze the optical properties by UV-visible spectrophotometer (UV-4802, Unico, China). Organic carbon for water extraction was detected by total organic analyzer (TOC-VCPH, Shimadzu). It should be noted that organic carbon for 90%DCM+10%MeOH extraction was measured by DRI Model 2001 Thermal/Optical Carbon Analyzer (Atmoslytic Inc., Calabasas, CA), following the IMPROVE A protocol. One portion of 90%DCM+10%MeOH extraction was concentrated in 0.5 mL, and then drawing 100 μL extracts into pretreatment filter. DCM and MeOH were removed by air dry, and then detected the remaining organic matters by thermal carbon analyzer.

For quality assurance and control, blank samples were processed by same procedure with actual samples, and all of the data were subtracted the value of blank sample. Moreover, every sample was detected three times to ensure the quality of data.

S2: Data process of mass absorption efficiency (MAE_{365})

Mass absorption efficiency (MAE) was defined as the optical absorption properties under the unit mass. (Yan et al., 2015) The equation for calculating the MAE_{365} was shown as followed:

$$MAE_{365,i}=(Abs_{\lambda})/[OC_i]=((ATN_{\lambda}-ATN_{700})*V_{w,i}/(Va*l)*\ln(10))/[OC_i] \quad (1)$$

Where $MAE_{365,i}$ is the mass absorption efficiency for solvent i extract at 365 nm ($m^2 \cdot g^{-1}$); $Abs_{\lambda\ is}$ light absorption coefficient (Mm^{-1}); [OCi] is the mass concentration of organic carbon for solvent i extract ($\mu g \cdot m^{-3}$); ATN_{λ} is the light attenuation at wavelength λ measured by the UV-visible spectrophotometer; $V_{w,i}$ is the volume of solvent i extract (mL); V_a is the air volume (m^3); and l is the optical length (0.01 m).

S3: Chemical characteristics of HULIS derived from two solvent extraction methods

In general, the chemical properties of extractions derived from water or DCM/MeOH were significantly different (**Fig. S1**). Some compounds with relatively low molecular weight and strong polarity of organic matter were extracted by water, while some with higher molecular weight and lower polarity of organic matter were left and then isolated by DCM/MeOH solvent extraction. For example, peaks derived from H_2O extractions for excavators under the working mode were predominantly of low molecular weight, with an average weight of 354±95 Da, while larger molecular weights were detected for DCM/MeOH extractions, with an average weight of 446±188 Da. Furthermore, O/C and DBE in H_2O extractions were higher than those in DCM/MeOH extractions (**Fig. S1**), indicating that the chemical species from the water solvent had a high degree of unsaturation and oxidation.

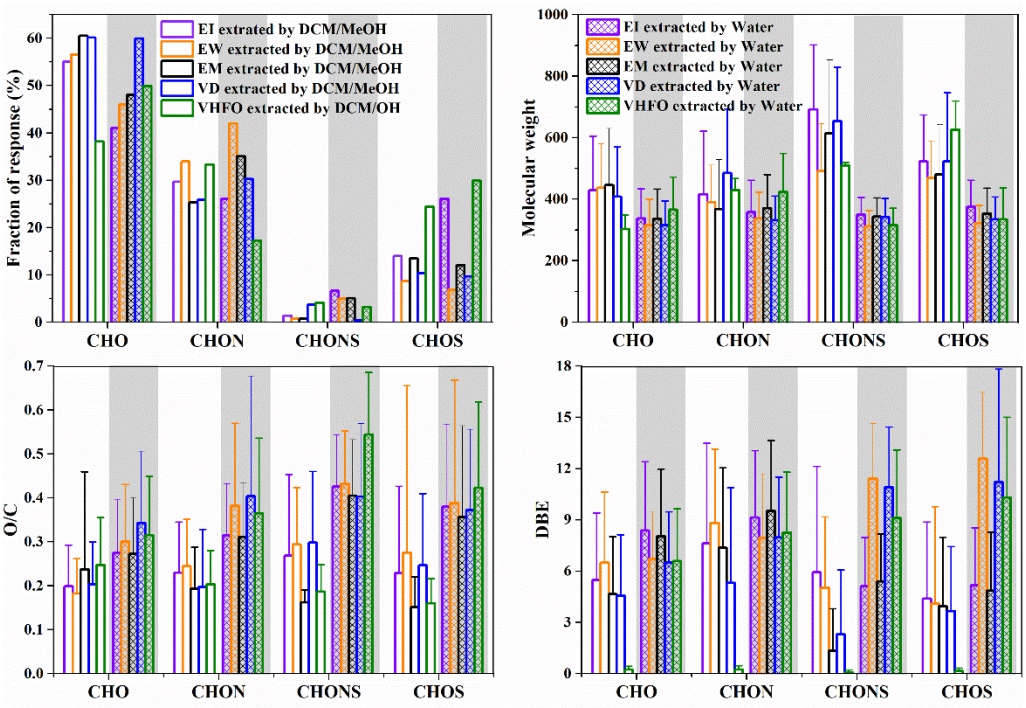

Figure S1 Differences in the fractions of response, molecular weight, O/C and DBE of

HULIS between water and DCM/MeOH extractions (EI is the excavator under idling mode; EW is the excavator under working mode; EM is the excavator under moving mode; VD is vessel using diesel and VHFO is vessel using heavy fuel oil).

Trends in relative elemental composition were consistent between the two solvent extractions, namely CHO>CHON>CHOS>CHONS. However, differences between samples for specific element groups or for off-road equipment were apparent (**Fig. S1**, **Fig. 1** and **Fig. S2**). The fraction of CHO group was higher for DCM/MeOH extraction than those for water extraction, while the rank of fractions of other N and S containing groups (CHON, CHONS and CHOS) between those two solvent extractions were reversed. For the CHON group, the highest fraction was observed for excavators under working mode, while the highest fraction of the CHOS group was for vessels using HFO, in both water and DCM/MeOH extractions.

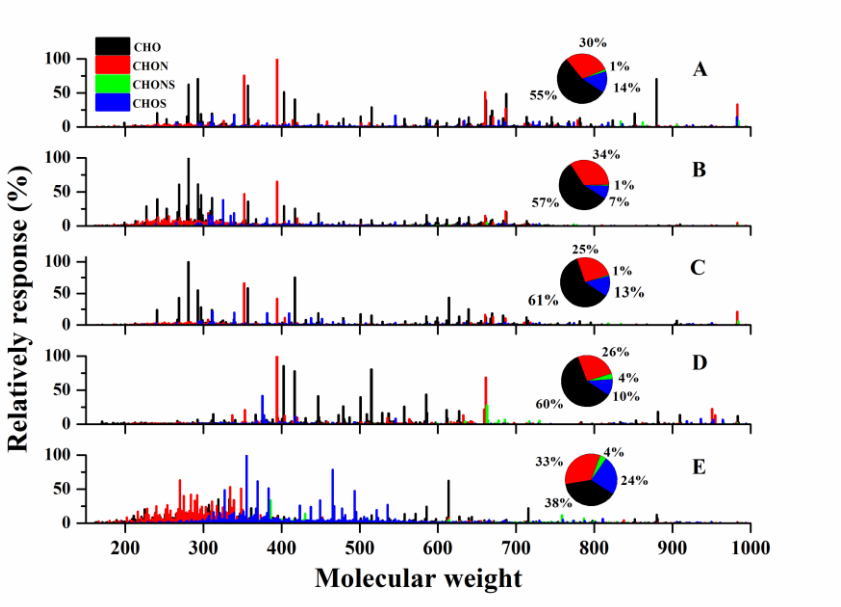

Figure S2 Mass spectrum of HULIS for off-road diesel engines. A, B, C, D and E were the mass spectra for excavators under idling, working, moving and vessels using diesel and heavy oil, respectively.

As shown in **Fig. S3**, trends for optical properties for water extraction of emissions from off-road engines were consistent with those identified for brown carbon within the UV-visible spectral region (<400 nm). Although the values of maximum optical attenuation for extractions by water and 90%DCM+10%MeOH were comparable, the average mass absorption efficiency of water extracts (0.95±0.21 m^2/g C for excavator and 0.83±0.29 m^2/g C for vessels) were significantly higher than those for 90% DCM+10% MeOH extracts (0.004±0.008 m^2/g C for excavator and 0.0005 m^2/g C for vessels using diesel). The $MAE_{365,\ wsoc}$ for off-road engines was slightly lower than those for crop straw burning and higher than those for wood burning and coal combustion.(Gelencs´er 2006, Mo et al., 2017, Wang et al., 2017) The different characteristics of mass spectra between H_2O and DCM/MeOH solvent extractions indicated that it was necessary to extract $PM_{2.5}$ by water to explore the emission characteristics of polar organic matters from off-road engines. In the following section, we discuss details about the chemical structure of compounds isolated using water extraction.

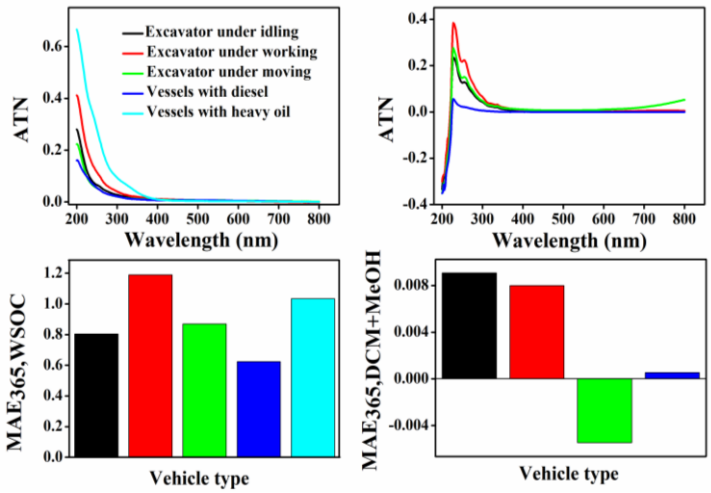

Figure S3 Absorption spectra measured by water (A and C) and 90%DCM+10%MeOH (B and D) extracts for off-road engines, respectively.

Table S1 Fractions of area of combined filters for samples to analyze the HULIS composition.

Samples / Filters	1[a]	2[a]	3[a]	4[a]	5[a]
YK	0.25	/	/	/	/
YF	0.25	/	/	/	/
GB1	/[b]	0.25	/	/	/
TB4	/	0.25	/	/	/
CAT320-I[c]	/	/	0.50	/	/
CAT320-M[c]	/	/	/	0.50	/
CAT320-W[c]	/	/	/	/	0.50
CAT330B-I	/	/	0.50	/	/
CAT330B-M	/	/	/	0.50	/
CAT330B-W	/	/	/	/	0.50
CAT307-I	/	/	0.50	/	/
CAT307-M	/	/	/	0.50	/
CAT307-W	/	/	/	/	0.50
PC60-I	/	/	0.50	/	/
PC60-M	/	/	/	0.50	/
PC60-W	/	/	/	/	0.50

a: The number of 1, 2, 3, 4, 5 represented the samples using for analyzing HULIS components; 1 and 2 represents the samples for vessels using heavy fuel oil and diesel, respectively; 3, 4 and 5 represented the samples for excavators under idling, moving and working modes, respectively;

b: "/" represented the samples didn't include this filter;

c: c, d and e represented the filters accessed from excavator emission under idling, moving and working modes, respectively.

Table S2 Characteristics of peaks observed in FT-ICR MS by water extraction for excavators and vessels.

Type	Group	Number of formula	Molecular weight		O/C		H/C		DBE		DBE/C	
			AVE	SD	AVE	SD	AVE	SD	AVE	SD	AVE	SD
Excavator (idling)	CHO	1746	338.0	96.69	0.28	0.12	1.18	0.35	8.40	4.03	0.44	0.18
	CHON	1488	358.8	102.97	0.32	0.12	1.14	0.33	9.17	3.91	0.49	0.17
	CHONS	334	349.8	57.43	0.43	0.12	1.46	0.30	5.13	2.86	0.34	0.15
	CHOS	1166	375.0	86.52	0.38	0.19	1.47	0.35	5.21	3.36	0.30	0.18
	Sum/Average	4734	355.4	85.90	0.35	0.14	1.31	0.33	6.98	3.54	0.39	0.17
Excavator (working)	CHO	1287	316.0	84.60	0.30	0.13	1.11	0.34	8.44	3.81	0.48	0.17
	CHON	1333	338.2	85.48	0.38	0.19	1.06	0.30	9.15	3.42	0.54	0.16
	CHONS	133	312.9	52.08	0.43	0.12	1.37	0.32	5.25	3.02	0.39	0.16
	CHOS	344	323.5	57.25	0.39	0.28	1.52	0.36	4.02	2.63	0.27	0.18
	Sum/Average	3097	322.6	69.85	0.38	0.18	1.26	0.33	6.71	3.22	0.42	0.17
Excavator (moving)	CHO	1797	336.7	96.57	0.27	0.13	1.21	0.35	8.07	3.94	0.42	0.18
	CHON	1969	371.4	108.84	0.31	0.12	1.14	0.32	9.56	4.11	0.49	0.17
	CHONS	284	344.1	60.43	0.41	0.13	1.42	0.30	5.41	2.79	0.36	0.15
	CHOS	681	353.9	81.98	0.36	0.21	1.49	0.36	4.86	3.45	0.29	0.18
	Average	4731	351.5	86.95	0.34	0.15	1.32	0.33	6.97	3.57	0.39	0.17
Excavator	CHO	1386	320.2	87.00	0.30	0.13	1.13	0.34	8.38	3.84	0.47	0.17
	CHON	1436	344.2	89.86	0.37	0.17	1.08	0.31	9.21	3.55	0.53	0.16
	CHONS	166	319.4	53.60	0.43	0.12	1.38	0.31	5.27	2.98	0.39	0.16
	CHOS	436	330.6	62.42	0.38	0.26	1.51	0.36	4.21	2.79	0.28	0.18
	Average	3424	328.6	73.22	0.37	0.17	1.27	0.33	6.77	3.29	0.42	0.17
Vessel (heavy oil)	CHO	1561	316.0	79.23	0.34	0.16	1.03	0.40	8.64	3.76	0.52	0.20
	CHON	1356	331.6	79.30	0.40	0.27	0.94	0.31	10.05	3.64	0.61	0.16
	CHONS	402	342.8	60.22	0.40	0.17	1.21	0.36	6.77	2.91	0.45	0.19
	CHOS	1235	334.7	72.86	0.37	0.18	1.25	0.46	6.58	4.33	0.41	0.23
	Average	4554	331.3	72.90	0.38	0.20	1.11	0.38	8.01	3.66	0.50	0.19
Vessel (diesel)	CHO	1318	308.7	85.76	0.31	0.14	1.15	0.37	7.72	3.83	0.45	0.19

	CHON	1144	343.1	102.35	0.33	0.16	1.14	0.35	8.81	4.14	0.50	0.18
	CHONS	13	462.8	168.97	0.37	0.18	1.39	0.65	10.08	11.91	0.36	0.32
	CHOS	343	313.1	136.65	0.38	0.17	1.45	0.41	6.05	6.52	0.31	0.21
	Average	2818	356.9	123.43	0.35	0.16	1.28	0.45	8.17	6.60	0.41	0.22
	CHO	1537	315.3	79.88	0.34	0.16	1.04	0.40	8.55	3.77	0.51	0.20
	CHON	1335	332.8	81.61	0.40	0.26	0.96	0.32	9.93	3.69	0.60	0.16
Vessel	CHONS	363	354.8	71.09	0.40	0.17	1.23	0.39	7.10	3.81	0.44	0.20
	CHOS	1146	332.5	79.24	0.37	0.18	1.27	0.46	6.53	4.55	0.40	0.23
	Sum/Average	4380	333.8	77.96	0.38	0.19	1.13	0.39	8.03	3.95	0.49	0.20

Table S3 The most abundant peaks of CHOS compounds emitted from excavators under three operation modes and diesel-fueled vessels.

	[M-H]⁻	m/z	DBE	Relative response (%)		[M-H]⁻	m/z	DBE	Relative response (%)
Excavator under idling	**$C_{16}H_{31}O_5S^-$**	335.1898	1	23.50	Excavator under moving	$C_5H_3O_{13}S_2^-$	334.902	4	11.95
	$C_{17}H_{33}O_5S^-$	349.2054	1	22.42		$C_4H_3O_{11}S_2^-$	290.9121	3	3.25
	$C_{15}H_{29}O_5S^-$	321.1741	1	22.07		$C_{22}H_{37}O_3S^-$	381.2469	4	3.02
	$C_{18}H_{35}O_5S^-$	363.2211	1	19.07		**$C_{14}H_{27}O_5S^-$**	307.1585	1	2.69
	$C_{14}H_{27}O_5S^-$	307.1585	1	16.28		**$C_{15}H_{29}O_5S^-$**	321.1742	1	2.64
	$C_{17}H_{35}O_5S^-$	351.2211	0	16.12		**$C_{16}H_{31}O_5S^-$**	335.1898	1	2.48
	$C_{16}H_{29}O_5S^-$	333.1741	2	14.63		**$C_{15}H_{27}O_5S^-$**	319.1585	2	2.37
	$C_{17}H_{31}O_5S^-$	347.1898	2	14.42		**$C_{18}H_{29}O_4S^-$**	341.1792	4	2.28
	$C_{18}H_{33}O_5S^-$	361.2054	2	14.39		**$C_{13}H_{25}O_5S^-$**	293.1428	1	2.07
	$C_{15}H_{27}O_5S^-$	319.1585	2	13.89		**$C_{16}H_{29}O_5S^-$**	333.1741	2	2.06
Excavator under working	$C_{22}H_{37}O_3S^-$	381.2469	4	33.63	Diesel-fueled vessel	$C_{12}H_{25}O_5S^-$	281.1428	0	22.20
	$C_{24}H_{41}O_3S^-$	409.2782	4	14.90		$C_{13}H_{27}O_5S^-$	295.1585	0	18.86
	$C_5H_3O_{13}S_2^-$	334.902	4	11.85		$C_{11}H_{23}O_5S^-$	267.1272	0	16.00
	$C_{16}H_{29}O_5S^-$	333.1741	2	8.43		**$C_{13}H_{25}O_5S^-$**	293.1428	1	15.57
	$C_{15}H_{27}O_5S^-$	319.1585	2	8.22		**$C_{15}H_{29}O_5S^-$**	321.1741	1	15.01
	$C_{16}H_{31}O_5S^-$	335.1898	1	7.89		**$C_{14}H_{27}O_5S^-$**	307.1585	1	14.75
	$C_{17}H_{31}O_5S^-$	347.1898	2	7.70		**$C_{12}H_{23}O_5S^-$**	279.1272	1	12.64
	$C_{15}H_{29}O_5S^-$	321.1741	1	7.58		**$C_{11}H_{21}O_5S^-$**	265.1115	1	11.14
	$C_{17}H_{33}O_5S^-$	349.2054	1	7.23		**$C_{16}H_{31}O_5S^-$**	335.1898	1	11.03
	$C_{14}H_{27}O_5S^-$	307.1585	1	6.77		**$C_{10}H_{19}O_5S^-$**	251.0959	1	8.74

The formulas marked with bold red color in Table S3 were the homologous compounds with $C_{12}H_{23}O_5S$- which was reported that generated from dodecane oxidation by Riva's research (Riva et al., 2016), while the formulas with bold blue color were likely formed from cycloalkanes.

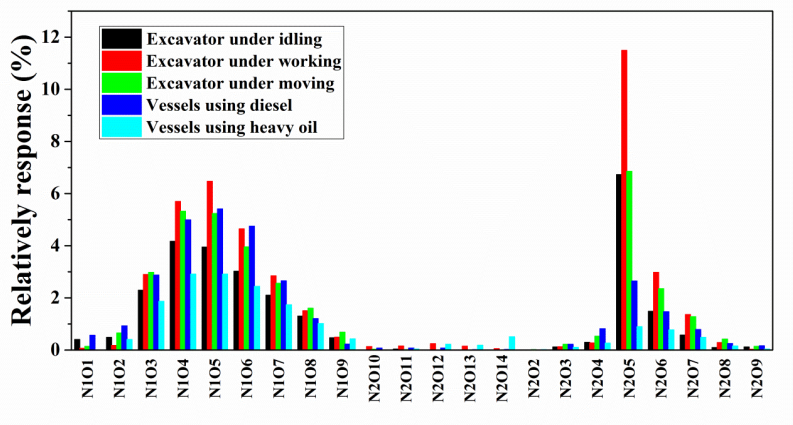

Figure S4 The distribution of subgroup of CHON for non-road vehicles

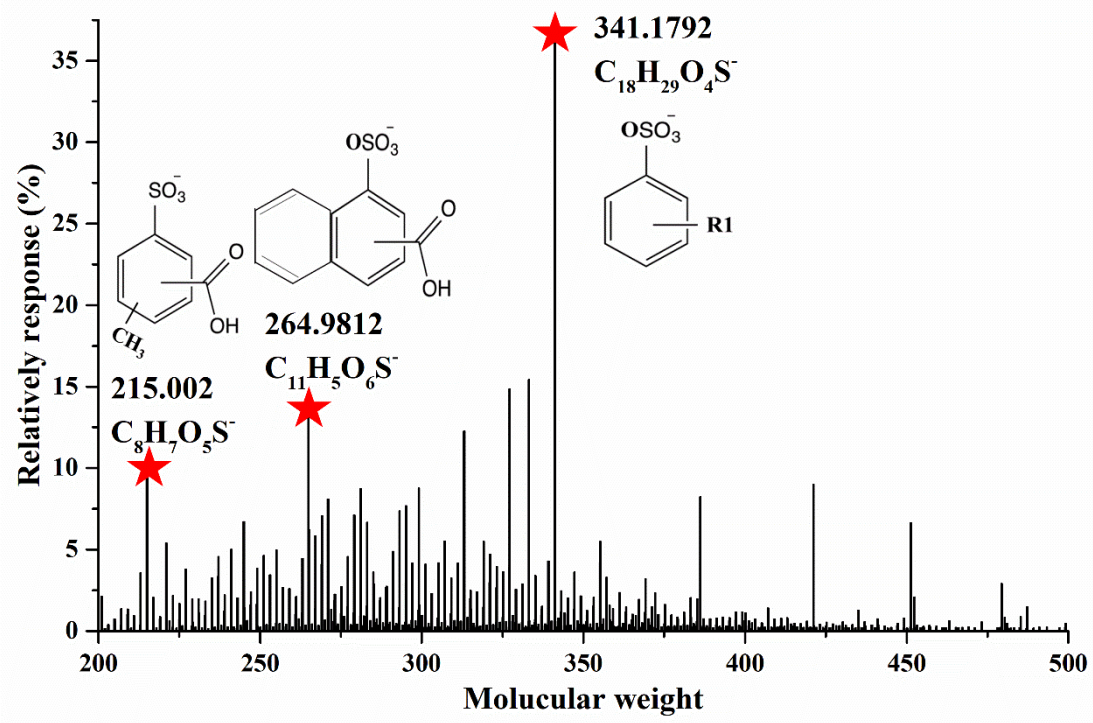

Figure S5 possible chemical structure of three of the most abundance peaks of S-containing compounds emitted from HFO-fueled vessels according to Riva et al., research (Riva et al., 2015).

Reference

Gelencs´er, M. O. A. a. A.: Black carbon or brown carbon? The nature of light-absorbing carbonaceous aerosols, 2006.

Mo, Y., Li, J., Liu, J., Zhong, G., Cheng, Z., Tian, C., Chen, Y. and Zhang, G.: The influence of solvent and pH on determination of the light absorption properties of water-soluble brown carbon, Atmospheric Environment, 161 (Supplement C): 90-98, 2017.

Riva, M., Tomaz, S., Cui, T., Lin, Y. H., Perraudin, E., Gold, A., Stone, E. A., Villenave, E., Surratt, J. D.: Evidence for an unrecognized secondary anthropogenic source of organosulfates and sulfonates: gas-phase oxidation of polycyclic aromatic hydrocarbons in the presence of sulfate aerosol, Environ Sci Technol, 49(11): 6654-6664, 2015.

Riva, M., Da Silva Barbosa, T., Lin, Y. H., Stone, E. A., Gold, A., Surratt, J. D.: Characterization of Organosulfates in Secondary Organic Aerosol Derived from the Photooxidation of Long-Chain Alkanes. Atmospheric Chemistry and Physics:1-39, 2016.

Wang, Y., Hu, M., Lin, P., Guo, Q., Wu, Z., Li, M., Zeng, L., Song, Y., Zeng, L., Wu, Y., Guo, S., Huang, X. and He, L.: Molecular Characterization of Nitrogen-Containing Organic Compounds in Humic-like Substances Emitted from Straw Residue Burning, Environmental Science & Technology, 51 (11): 5951-5961, 2017.

Yan, C., Zheng, M., Sullivan, A. P., Bosch, C., Desyaterik, Y., Andersson, A., Li, X., Guo, X., Zhou, T., Gustafsson, Ö. and Collett, J. L.: Chemical characteristics and light-absorbing property of water-soluble organic carbon in Beijing: Biomass burning contributions, Atmospheric Environment, 121 (Supplement C): 4-12, 2015.